

GraphPilot: Grounded Scene Graph Conditioning for Language-Based Autonomous Driving

Fabian Schmidt^{1,2} MarkusENZweiler¹ Abhinav Valada²

¹Esslingen University of Applied Sciences ²University of Freiburg

Abstract

Vision-language models have recently emerged as promising planners for autonomous driving, where success hinges on topology-aware reasoning over spatial structure and dynamic interactions from multimodal input. However, existing models are typically trained without supervision that explicitly encodes these relational dependencies, limiting their ability to infer how agents and other traffic entities influence one another from raw sensor data. In this work, we bridge this gap with a novel model-agnostic method that conditions language-based driving models on structured relational context in the form of traffic scene graphs. We serialize scene graphs at various abstraction levels and formats, and incorporate them into models via structured prompt templates, enabling systematic analysis of when and how relational supervision is most beneficial and computationally efficient. Extensive evaluations on the LangAuto and Bench2Drive benchmarks show that scene graph conditioning yields large and persistent improvements. We observe a substantial performance increase in the Driving Score of our proposed approach versus competitive LMDrive, BEVDriver, and SimLingo baselines. These results indicate that diverse architectures can effectively internalize and ground relational priors through scene graph-conditioned training, even without requiring scene graph input at test-time. Code, fine-tuned models, and our scene graph dataset are publicly available at <https://github.com/iis-esslingen/GraphPilot>.

1. Introduction

Understanding complex traffic scenes remains a central challenge in autonomous driving, especially when decision-making is conditioned on natural language instructions [4]. Modern language-based driving agents operate at the intersection of perception, language, and planning, requiring not only accurate scene understanding but also the ability to reason about spatial structure, traffic rules, and interactions among dynamic actors [49]. While recent works have shown that vision-language models (VLMs) can map

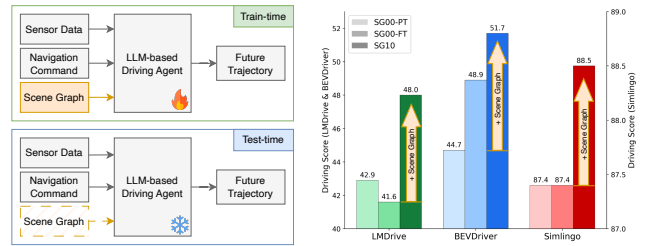


Figure 1. **Explicit relational grounding through scene graph conditioning.** We visualize three setups: SG00-PT (the original pretrained baseline), SG00-FT (the baseline fine-tuned without scene graphs), and SG10 (conditioned on scene graphs during training but absent at test-time). The significant performance gains across LMDrive, BEVDriver, and SimLingo suggest that models internalize relational structure during training, even when scene graphs are absent at test-time.

image and language inputs to plausible trajectories [33–36, 48, 57, 58], their performance in complex environments remains limited. A key limitation is that current models typically rely on representations that do not explicitly encode relational structure, forcing them to infer safety-critical interactions implicitly from dense features [56].

Scene graphs provide a structured solution to this limitation [18, 19]. By explicitly representing a traffic scene as a structured graph of entities and their relations, they encode not only *what* is present in the environment, but also *how* entities are related and may influence one another. In scene graphs, nodes represent objects such as vehicles, pedestrians, traffic lights, and roadway elements, while edges express spatial, semantic, and regulatory relations, e.g., which vehicle is in which lane, which traffic light controls which direction, and how nearby actors might interact. This structured relational view enhances semantic understanding and enables more informed planning [3].

Despite their growing use in indoor navigation and instruction-following tasks [10, 13, 30, 32, 47, 52], scene graphs have only recently gained attention in outdoor autonomous driving, mainly for tasks such as risk estimation [24, 27], and trajectory prediction [16, 59]. However, their integration into language-based planning remains unexplored. Instead, most existing systems represent the scene

using dense geometric or visual features, including image tokens [33, 57, 58] or BEV grids [12, 36, 48], followed by generic attention mechanisms. As a result, critical relationships between entities must be inferred implicitly. This gap motivates our central question: Can *explicit* relational structure of a traffic scene help language-based driving models internalize and reason over spatial and causal dependencies in traffic scenes?

To address this question, we introduce a model-agnostic approach for injecting structured semantic context into language-based autonomous driving systems. We construct traffic scene graphs at each time step and serialize them into human-readable formats (text, JSON, YAML), which are then provided to the language model along with the navigation instruction and sensory input, as shown in Fig. 1. We make this a deliberate design choice to avoid changes to the model architecture, additional training objectives, or specialized graph encoders, thereby maintaining model-agnostic applicability and ease of integration. This is the first work to inject a traffic scene graph as explicit context for planning in a language-based driving model.

Our experiments reveal several key insights. First, employing scene graph prompts at test-time alone improves performance over the original models. Second, training with scene graph supervision yields significant gains in driving performance, and importantly, these improvements persist even when scene graphs are omitted at test-time. This indicates that language-based planners can internalize structured relational knowledge during training and leverage it without explicit relational input at inference. Finally, we find that leaner scene graph abstractions offer a strong trade-off between semantic fidelity and prompt efficiency, achieving high performance with fewer tokens.

Our main contribution is a model-agnostic training paradigm that grounds language-based autonomous driving models in explicit relational structure via serialized traffic scene graphs. Specifically, our contributions are three-fold: (i) **Model-agnostic relational grounding**, as we propose the first approach to inject structured traffic scene graphs into vision-language planners without requiring architectural changes or specialized encoders. (ii) **Relational internalization**, where we identify a novel paradigm in which models internalize spatial and causal dependencies during training to achieve significant performance gains even when scene graphs are absent at test-time. (iii) **Efficient scene representation**, where we define a hierarchy of abstractions and serialization formats that identify the most token-efficient representations for planning without sacrificing driving performance. We systematically validate these contributions across multiple state-of-the-art models (LMDrive, BEVDriver, SimLingo) to demonstrate the universal benefit of explicit relational conditioning.

2. Related Work

We discuss related work regarding (1) language-based autonomous driving, where VLMs are used to plan from multimodal inputs and instructions, and (2) traffic scene graphs, which provide structured driving scene representations.

Language-Based Autonomous Driving: We review language-driven methods for trajectory planning and decision making in autonomous driving, covering both open-loop waypoint prediction on nuScenes [1] and closed-loop evaluation using CARLA [6] or NavSim [5]. Several works deploy VLMs as planners, mapping sensor data and navigation commands directly to a sequence of future waypoints [33, 36, 48, 50, 51, 58]. LMDrive [36] presents a VLM-based end-to-end stack that fuses camera and LiDAR inputs with a natural-language navigation command. BEVDriver [48] extends this design by strengthening the vision encoder to produce richer BEV features, improving semantic and spatial grounding. Beyond direct waypoint prediction, some approaches aim to increase reasoning fidelity by incorporating chain-of-thought within a perception-prediction-planning paradigm, accepting additional latency in exchange for interpretability and more transparent decision making [15, 20, 38, 54]. Efficiency-oriented systems activate the language model only when it is expected to contribute: AdaDrive [57] learns an adaptive slow-fast collaboration that decides when and to what extent the VLM should be involved. Other approaches decouple high-level reasoning from trajectory generation. Here, the VLM proposes subgoals, constraints, or safety checks, and a non-VLM planner converts these signals into concrete trajectories [2, 7, 11, 31]. ORION [7], for example, predicts planning tokens with an LLM and conditions a generative planner on these tokens to produce multi-modal trajectories. Finally, several approaches transfer the world-knowledge and reasoning capabilities of VLMs into training-time supervision, thereby removing the need for an online VLM at inference while retaining its benefits [12, 55]. In parallel, retrieval-augmented (RAG) methods condition decisions on similar scenarios or past experiences to improve robustness on rare or long-tail events [28, 45, 46, 53, 56].

Scene Graphs in Autonomous Driving: Traffic scene graphs represent road users, roadway structure, and their relations as a graph. Research spans multiple directions: construction from sensory and map data, safety and risk estimation, semantic scene retrieval, and trajectory prediction. On the construction side, recent work builds scene graphs from video, multi-camera perception, and HD maps, progressing from rule-based extractors to learned relation predictors and lane-topology transformers, and further to multi-agent 3D urban scene graphs [9, 25, 26, 37, 39, 42, 44, 60]. This shift reflects a move away from hand-crafted priors toward a data-driven structure that adapts to diverse traf-

fic layouts and interaction patterns. For safety reasoning, scene graphs enable spatio-temporal modeling of interactive dynamics with multi-relational GNNs and sequence models, supporting early collision prediction and pedestrian risk assessment [24, 26, 27, 61]. For retrieval and downstream decision support, methods based on subgraph matching, together with hybrids that use VLM-generated descriptions, identify semantically similar scenes, mine failure patterns, and return mitigation knowledge to the planner through RAG-style augmentation [22, 40–42]. Graph-based trajectory prediction approaches model interactions among agents and their surrounding map context, using graph- or transformer-based encoders to capture spatial and relational dependencies for subsequent motion forecasting [16, 29, 59, 62]. Unlike prior work, we are the first to serialize the scene graph and incorporate it directly into a language-based driving model as auxiliary context for decision-making and planning.

Scene Graphs in Autonomous Driving: Traffic scene graphs represent road users, roadway structure, and their relations as a graph. Research spans multiple directions: construction from sensory and map data, safety and risk estimation, semantic scene retrieval, and trajectory prediction.

On the construction side, recent work builds scene graphs from video, multi-camera perception, and HD maps, progressing from rule-based extractors to learned relation predictors and lane-topology transformers, and further to multi-agent 3D urban scene graphs [9, 25, 26, 37, 39, 42, 44, 60]. This shift reflects a move away from hand-crafted priors toward data-driven structure that adapts to diverse traffic layouts and interaction patterns. For safety reasoning, scene graphs enable spatio-temporal modeling of interactive dynamics with multi-relational GNNs and sequence models, supporting early collision prediction and pedestrian risk assessment [24, 26, 27, 61]. For retrieval and downstream decision support, methods based on subgraph matching, together with hybrids that use VLM-generated descriptions, identify semantically similar scenes, mine failure patterns, and return mitigation knowledge to the planner through RAG-style augmentation [22, 40–42]. Graph-based trajectory prediction approaches model interactions among agents and their surrounding map context, using graph- or transformer-based encoders to capture spatial and relational dependencies for subsequent motion forecasting [16, 29, 59, 62]. Distinct from prior work, we are the first to serialize the scene graph and incorporate it directly into a language-based driving model as auxiliary context for decision making and planning.

3. Method

Our method conditions a language-based model on serialized traffic scene graphs to enable structured reasoning for downstream driving decisions.

3.1. Scene Graph Construction

We first construct a scene graph for each time step by detecting nodes and extracting relations, building on [26].

Formalization. We represent the scene at time t as a directed, labeled multigraph $G_t = (V_t, E_t, \mathcal{R})$, where V_t is the set of nodes, $E_t \subseteq V_t \times \mathcal{R} \times V_t$ the set of labeled edges, and \mathcal{R} the relation vocabulary, cf. Fig. 2.

Nodes carry a unique identifier as well as a semantic class and are organized into three disjoint groups: (i) structural nodes \mathcal{S}_t , (ii) actor nodes \mathcal{A}_t , and (iii) traffic-related objects \mathcal{O}_t , so that $V_t = \mathcal{S}_t \cup \mathcal{A}_t \cup \mathcal{O}_t$. Structural nodes encode the static roadway scaffold, i.e., *lanes*, *roads*, and *junctions*, which provide the spatial context and connectivity for motion. Actor nodes represent road users, including the *ego* vehicle, which is always present, and other participants such as light vehicles (*car*, *van*, *taxi*, *electric vehicle*), heavy vehicles (*truck*, *bus*), *motorcycle*, *bicycle*, *emergency vehicles*, and *pedestrian*. These entities and their interactions define the scene dynamics that govern the ego vehicle’s driving decisions. Traffic-related objects capture regulatory context, for example *traffic light*, *speed limit*, and *stop sign*, which constrain admissible behavior and help anticipate required maneuvers such as stopping or yielding.

The relation vocabulary \mathcal{R} is partitioned into six semantic groups. Proximity relations (*safety hazard*, *near collision*, *super near*, *very near*, *near*, *visible*) quantify distance- and risk-based interactions that are key for collision avoidance. Directional relations (*direct front*, *side front*, *direct rear*, *side rear*) describe longitudinal ordering and approach geometry that affect yielding, following, or braking decisions. Lateral relations (*left of*, *right of*) encode side-by-side context that is essential for lane keeping and safe lane changes. The hierarchical relation (*is in*) anchors actors and objects within their structural context, thereby localizing rules and right-of-way. Topological relations (*opposes*, *travels to*, *lane change*) define lane graph connectivity, while regulatory relations (*controls traffic of*) link traffic devices to the structural elements they govern.

We impose lightweight typing constraints on which node classes may be connected by which relations to ensure a compact and consistent graph. The hierarchical assignment builds the scene hierarchy by linking actors to lanes, lanes to roads, and, when present, roads to junctions via *is in*. The ego connects directly to its lane via *is in*, and ego-actor interactions are restricted to behaviorally relevant geometry, so only proximity, directional, and lateral relations are instantiated between actor pairs. Regulatory edges apply only to traffic lights and connect a *traffic light* node to the lanes it governs via *controls traffic of*. We do not add regulatory edges for speed limits or stop signs. Lane-to-lane relations capture the network structure and include topological and lateral relations.

Abstraction Levels. Beyond the full graph, we introduce

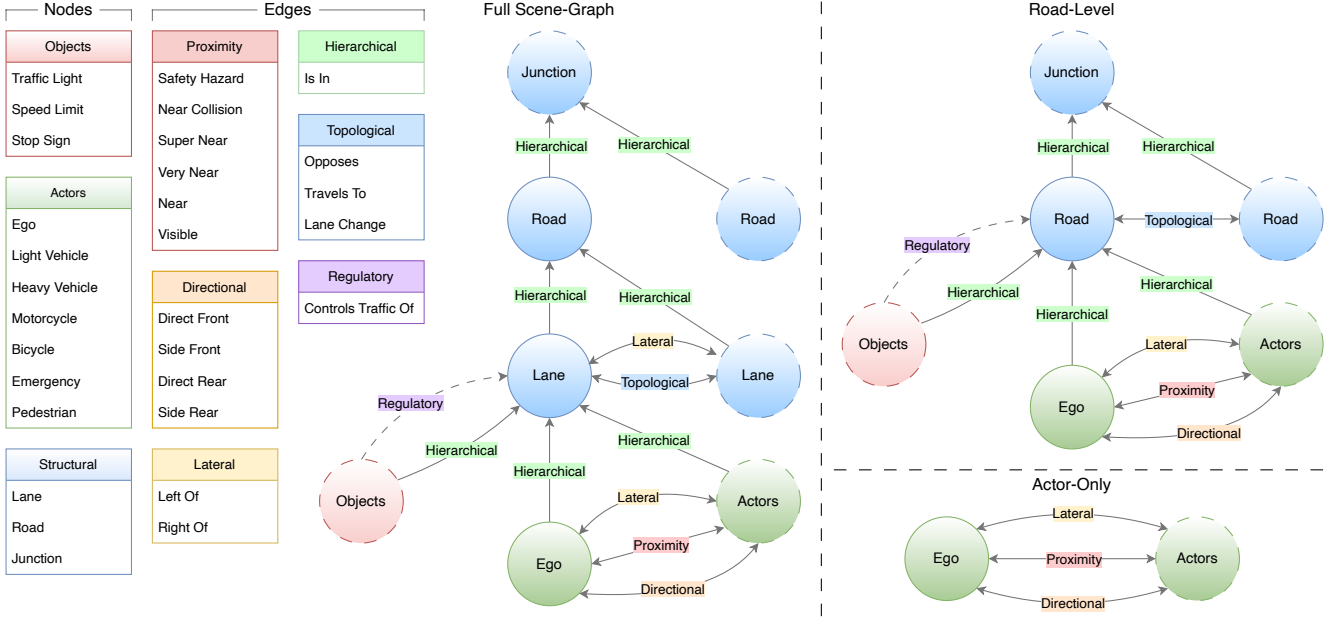


Figure 2. **Scene graph construction.** Each traffic scene is represented as a structured, labeled graph capturing entities (actors, objects, structure) and their relations. We define three levels of abstraction: *Full* (all node types and relations), *Road-Level* (collapsed structural detail), and *Actor-Only* (actors and their pairwise interactions), enabling analysis of the trade-off between relational fidelity and prompt efficiency. Dashed nodes and edges indicate optional elements that are not always present.

two abstractions to identify which structural components contribute most to planning performance, while reducing prompt length and sensitivity to extraction noise, and quantifying the trade-off between efficiency and fidelity.

Road-Level collapses fine-grained lane nodes into parent roads. It aggregates lane-level relations such as actor-road membership and *travels to* topological edges to the road graph while removing lane-specific relations like *lane change*. This reduction isolates whether high-level road geometry suffices for planning compared to dense lane-level data. The second abstraction *Actor-Only* removes structural and object nodes altogether and retains only the ego and other actors with their pairwise spatial and directional relations. By removing hierarchical, topological, and regulatory edges, this variant restricts the scene graph context to local inter-actor geometry to assess its contribution to the planning signal.

3.2. Scene Graph Serialization

We serialize each graph as subject-predicate-object statements using a fixed, human-readable relation vocabulary. Fig. 3 illustrates the three formats we use, i.e., Text, JSON, and YAML, and a concrete example for each. To avoid redundancy, multiple predicates between the same ordered pair (s, o) are emitted once as a multi-label statement rather than as duplicated links. When linearized, we list statements in hierarchical order with roads to junctions, lanes to roads, lane to lane connectivity, objects to lanes, and actors

to lanes, and finally interactions between actors.

Text. The Text form is a compact, linearized sequence of statements separated by a vertical bar (`|`). It applies two packing rules: First, *membership grouping* aggregates multiple sources that share the same hierarchical target, yielding “ s_1, s_2 is in o ”. Second, *predicate merging* collects all predicates that hold for a fixed ordered pair, yielding “ s p_1, p_2, \dots o ”. Statements are emitted in a fixed order with hierarchical assignments first and actor-actor interactions following.

Structured Formats (JSON/YAML). Both formats mirror the graph using two collections: *nodes* (storing *id* and *base_class*) and *links*. To ensure a compact schema, each link represents a unique ordered pair (s, o) and aggregates all applicable predicates into a single *labels* list. While JSON provides a standard parser-friendly structure, YAML uses indentation-based nesting, which yields a more token-efficient representation by omitting braces and quotes.

3.3. Scene Graph Injection

We instantiate three prompt templates that differ in layout and instruction framing while keeping the underlying content identical. Fig. 4 shows all three templates side by side for direct comparison. The first template (*VI*) concatenates the navigation command and the scene graph in a single line without section headers. The command appears first, followed by a short cue and the serialized graph. This variant minimizes prompt overhead and matches the instruction-

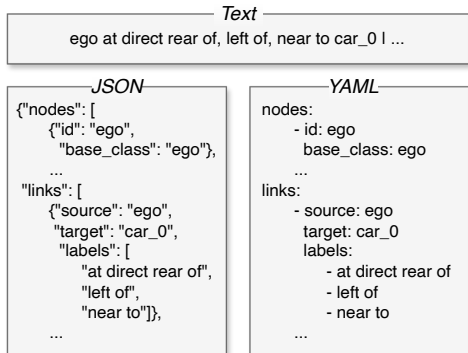


Figure 3. **Serialization formats.** We serialize scene graphs as Text, JSON, or YAML, each encoding subject-predicate-object triplets.

plus-context compositions observed in prior work. The second template (V2) introduces explicit section headers for the scene graph and for the navigation command and begins with a reminder that the model acts as the ego vehicle. The graph is shown as a headed block and the command as a separate headed block, which makes both inputs distinct and separable when contexts become longer. The third template (V3) keeps the sectioning and wraps the scene graph in a fenced block with a format prefix such as `text`, `json`, or `yaml`. It also states a short *Primary Objective* that emphasizes adherence to the external navigation command. The fence treats the graph as read-only and aims to stabilize tokenization for larger graphs or mixed formatting, and the format prefix encourages consistent parsing across representations.

3.4. Scene Graph Conditioning

We condition the model on structured relational information by including a serialized scene graph alongside the natural-language navigation command in the input prompt. In this work, we use the term *conditioning* to refer specifically to prompt-level supervision: the model receives explicit relational context as part of its input, but its architecture, training objective, and loss functions remain unchanged. This prompt-based conditioning allows the model to ground decision-making and planning in spatial topology, regulatory context, and inter-actor interactions that would otherwise need to be inferred implicitly from visual features alone. Since scene graph-conditioning operates purely at the input level, it is model-agnostic and does not require modifying perception modules, introducing graph encoders, or defining auxiliary training losses.

4. Experiments

We evaluate the impact of scene graph-conditioning on VLM-based autonomous driving systems across multiple configurations and training setups.

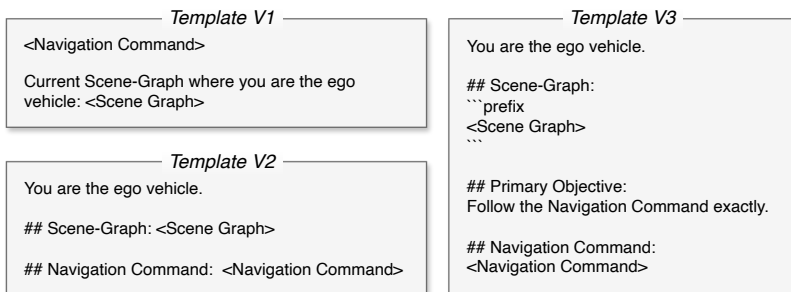


Figure 4. **Prompt templates.** Three prompt templates combine scene graphs with navigation commands: V1 uses direct concatenation, V2 adds ego-role framing and section headers, and V3 introduces a structured preamble with markdown-style fencing for consistent formatting.

4.1. Benchmark

We evaluate our approach on two CARLA-based [6] closed-loop benchmarks: LangAuto [36] and Bench2Drive [17]. LangAuto adapts the CARLA Leaderboard for language-based driving across eight towns, featuring diverse traffic, weather, and illumination conditions, in which discrete goal points are replaced by natural-language instructions. Bench2Drive utilizes 220 short routes, approximately 150m each, spanning 44 interactive scenarios with five routes per scenario across 15 towns to evaluate state-of-the-art driving agents.

Metrics. For both benchmarks, we report the official Driving Score (DS), defined as the product of Route Completion (RC) and the Infraction Score (IS). RC measures the fraction of the route distance achieved, while IS applies multiplicative penalties for traffic-rule violations and collisions. We also report the Success Rate (SR) for Bench2Drive, which measures the proportion of routes successfully completed. Following standard protocols, all results are averaged across three execution seeds.

4.2. Baselines

We evaluate our approach using three state-of-the-art VLM-based driving systems: LMDrive [36] (LLaVA-v1.5 [23]) and BEVDriver [48] (LLaMA-7B [43]) for LangAuto, and SimLingo [33] (InternVL2-1B [8]) for Bench2Drive. These baselines represent diverse architectural paradigms, allowing us to demonstrate the broad applicability of our method across different vision-language foundations. Following standard protocols, all baselines are evaluated using their officially released model variants to ensure a fair comparison.

Dataset Collection. The publicly available LMDrive and SimLingo datasets do not include scene graphs. Therefore, we extend the official data generation pipelines with our scene graph generation, abstraction, and serialization modules so that ground-truth scene graphs are captured along-

side the original modalities. These graphs are constructed from privileged simulator state by utilizing 3D bounding boxes and HD map metadata to ensure high-fidelity relational labels. While our pipeline is implemented for CARLA, this approach remains directly applicable to real-world datasets (e.g., nuScenes) where such annotations are standard. The resulting data preserves the original distribution over selected routes, towns, weather, and illumination, and remains fully compatible with the original frameworks. We utilize our extended LMDrive dataset to train LMDrive and BEVDriver, while the extended SimLingo dataset is used to train SimLingo.

4.3. System Configurations

For our approach, we define four scene graph usage settings, i.e., SG00, SG01, SG10, and SG11, to evaluate the impact of relational supervision on driving. SG00 uses no scene graphs during training or test-time and serves as our main baseline. We distinguish between two variants: SG00-PT uses the original pretrained checkpoints provided by the model authors, while SG00-FT further fine-tunes these checkpoints on our collected dataset. This distinction ensures a fair comparison, as directly comparing our scene graph-conditioned models to SG00-PT would conflate the effects of additional training data with those of scene graph supervision. SG01 includes scene graphs only at test-time. This setting probes whether pretrained models can benefit from relational structure without any prior exposure to scene graphs during training. SG10 includes scene graphs during training but omits them at test-time. This measures whether models can internalize relational priors and generalize without needing explicit scene graph input during inference. SG11 includes scene graphs at both training and test-time and represents the fully supervised scenario.

4.4. Implementation Details

We initialize all models from officially released checkpoints and strictly adhere to the optimization protocols provided by each baseline. While all models train their respective projection layers and action heads, they differ in their primary backbones: LMDrive keeps both the vision encoder and language model frozen while training the Q-Former [21]; BEVDriver freezes the vision encoder but trains the LLM via LoRA [14] and the Q-Former; and SimLingo utilizes a fully trainable vision encoder alongside a LoRA-optimized language backbone. We maintain these original training recipes without additional losses or auxiliary tasks. By ensuring that all components outside the prompt remain unchanged, performance gains are strictly attributable to the internalized relational knowledge of our scene graphs, rather than to architectural modifications.

4.5. Training

All models are trained on eight NVIDIA L40s GPUs for five epochs using the original train/validation splits. Scene graphs (SG10/SG11) are integrated via the prompt based on the selected abstraction and serialization without altering the underlying model architecture. Total training time depends primarily on the baseline architecture and serialization format, with Text being significantly more efficient than the verbose JSON format. Specifically, training ranges from 20h (AO, Text) to 29h (AO, JSON) for SimLingo. For BEVDriver, durations range from 34h (AO, Text) to 78h (Full, JSON), while LMDrive requires 61h (AO, Text) to 106h (Full, JSON). The choice of injection template has a negligible effect on training efficiency.

4.6. Results and Ablations

Zero-Shot Test-Time Scene Graph Injection (SG01). We begin by evaluating which scene graph integration strategies are most effective when applied at test-time only, without additional training, to assess whether a pretrained model can benefit from relational context without prior explicit conditioning. This analysis identifies the optimal configuration for subsequent experiments.

Specifically, we evaluate all combinations of abstraction level, serialization format, and injection template. Tab. 1 reports DS, RC, and IS for LMDrive averaged over the LangAuto *Tiny*, *Short*, and *Long* tracks. We provide mean rows and columns to facilitate comparisons across serialization formats and injection templates. Notably, multiple test-time configurations already surpass the performance of the original pretrained baselines, underscoring the inherent potential of relational grounding even without fine-tuning. Two consistent trends emerge from this zero-shot evaluation. First, injection template V3 consistently outperforms V2 and V1, with V1 trailing significantly. Second, Actor-Only abstractions yield the best results across all formats, indicating that minimal but structured relational information is most beneficial for pretrained models. These findings highlight the strength of lean representations. Actor-Only graphs strike a favorable balance between semantic relevance and token budget by introducing the fewest additional tokens, as depicted in Fig. 5. Based on these insights, we select the Actor-Only abstraction and injection templates V2 and V3 for all subsequent fine-tuning experiments, focusing on configurations that maximize prompt efficiency and clarity.

Knowledge Internalization (SG10). Tab. 2 reports the driving performance for our SG10 configurations using the optimal Actor-Only abstraction and injection templates (V2, V3). To ensure fair, environment-matched comparisons, we reproduce all results on our local hardware using the original pretrained baselines (SG00-PT) and models fine-tuned without scene graphs (SG00-FT). This setup allows us to assess the extent to which structured relational

Table 1. **Zero-shot test-time scene graph injection (SG01)**. Results for the pretrained LMDrive model across abstraction levels, formats, and templates. Results are averaged across LangAuto Tiny, Short, and Long. The rightmost column shows the mean token count for each configuration on the LMDrive dataset.

Serial.	Abstract.	V1			V2			V3			Mean			Tokens
		DS \uparrow	RC \uparrow	IS \uparrow	DS \uparrow	RC \uparrow	IS \uparrow	DS \uparrow	RC \uparrow	IS \uparrow	DS \uparrow	RC \uparrow	IS \uparrow	
Text	Full	38.9	46.2	0.84	41.3	49.7	0.83	41.8	49.4	0.83	40.7	48.4	0.83	437
	Road-Level	40.6	47.0	0.86	40.5	50.1	0.81	41.5	49.4	0.83	40.9	48.8	0.83	370
	Actor-Only	40.0	48.7	0.85	43.1	51.2	0.84	44.7	53.0	0.84	42.6	51.0	0.84	69
JSON	Full	34.6	42.2	0.84	41.5	48.7	0.84	44.6	54.6	0.83	40.2	48.5	0.84	2905
	Road-Level	34.4	43.4	0.83	41.8	51.2	0.81	46.6	56.3	0.82	41.0	50.3	0.82	2172
	Actor-Only	40.3	47.3	0.85	42.6	52.3	0.82	44.7	55.6	0.82	42.6	51.7	0.83	409
YAML	Full	39.4	45.5	0.85	41.8	50.4	0.82	41.8	51.9	0.80	41.0	49.3	0.82	1712
	Road-Level	39.2	46.6	0.85	41.8	51.5	0.82	42.1	50.6	0.83	41.1	49.6	0.83	1246
	Actor-Only	42.8	52.0	0.84	43.6	53.2	0.82	44.7	52.7	0.84	43.7	52.6	0.83	242
Mean	Full	37.6	44.6	0.84	41.5	49.6	0.83	42.7	52.0	0.82	40.6	48.3	0.83	
	Road-Level	38.1	45.7	0.84	41.4	50.9	0.81	43.4	52.1	0.83	41.0	49.6	0.83	
	Actor-Only	41.1	49.4	0.85	43.1	52.2	0.82	44.7	53.8	0.83	43.0	51.8	0.84	

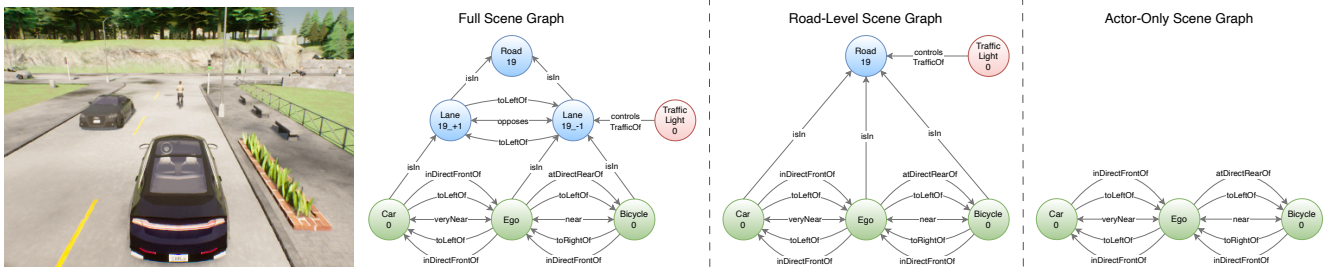


Figure 5. **Scene graph abstractions**. Comparison of Full, Road-Level, and Actor-Only abstractions, demonstrating how structural detail is progressively filtered.

context is internalized during training to benefit test-time, where graphs are absent.

For LMDrive, our SG10 approach consistently outperforms both the pretrained baseline and the standard fine-tuning setup. The best configuration (Text, V3) achieves a DS of 51.8, marking a substantial improvement over the baseline (42.9) and the SG00-FT variant (41.5). Notably, these results significantly surpass the best zero-shot SG01 performance (44.7) previously shown in Tab. 1, demonstrating that explicit training with relational supervision is more effective than simple test-time injection. BEVDriver shows a similar trend of significant improvement. The top configuration (YAML, V2) reaches a DS of 56.1, outperforming its respective SG00-PT (44.7) and SG00-FT (48.9) benchmarks. While BEVDriver shows a preference for YAML serialization and the V2 template, the underlying pattern remains consistent with LMDrive: training-time scene graph exposure enhances internal planning behavior even when that structure is removed during deployment. To demonstrate that these benefits are not specific to the LangAuto benchmark, we further evaluate our strategy using SimLingo on the Bench2Drive dataset. Despite a high base-

line performance of 87.4, SimLingo achieves consistent improvements across all formats, with the best configuration (JSON, V2) reaching a DS of 88.9. We hypothesize that scene graph supervision acts as a relational bottleneck during training. By forcing the model to predict actions conditioned on explicit subject-predicate-object triplets, the vision-language backbone (e.g., the Q-Former or LoRA-tuned LLM) learns to prioritize safety-critical spatial features and dynamic inter-actor dependencies. Consequently, the model "learns to attend" to these relational cues within the raw sensory input, allowing the internalized reasoning logic to persist even when the text-based scene graph is removed at test-time. This SG10 strategy offers major practical advantages: it eliminates complex and potentially error-prone test-time scene graph generation and reduces prompt length, significantly lowering the computational and memory load essential for real-time systems.

Extended Infraction Analysis. To better understand how scene graph conditioning influences safety, we analyze detailed sub-metrics in Tab. 3, averaging over all V3-based LMDrive configurations. Compared to the original baseline (SG00-PT), SG10 yields significant reductions in crit-

Table 2. **Knowledge internalization (SG10)**. Performance of our SG10 strategy across LMDrive, BEVDriver, and SimLingo using Actor-Only graphs compared to pretrained (SG00-PT) and fine-tuned (SG00-FT) baselines.

Config.	LMDrive						BEVDriver						SimLingo			
	V2			V3			V2			V3			V2		V3	
	DS ↑	RC ↑	IS ↑	DS ↑	RC ↑	IS ↑	DS ↑	RC ↑	IS ↑	DS ↑	RC ↑	IS ↑	DS ↑	SR ↑	DS ↑	SR ↑
SG00-PT	42.9	54.8	0.80	42.9	54.8	0.80	44.7	49.7	0.90	44.7	49.7	0.90	87.4	0.72	87.4	0.72
SG00-FT	41.5	48.2	0.88	41.5	48.2	0.88	48.9	56.4	0.86	48.9	56.4	0.86	87.4	0.71	87.4	0.71
Text	46.8	56.2	0.84	51.8	59.4	0.86	51.7	59.8	0.87	51.5	60.0	0.86	88.4	0.72	88.1	0.71
JSON	45.7	53.5	0.85	45.5	54.0	0.85	47.3	52.1	0.90	42.2	50.7	0.85	88.9	0.73	88.4	0.72
YAML	47.9	57.4	0.83	46.8	54.8	0.84	56.1	64.1	0.87	48.2	55.7	0.85	88.2	0.71	87.9	0.70
Mean	46.8	55.7	0.84	48.0	56.1	0.85	51.7	58.7	0.88	47.3	55.5	0.85	88.5	0.72	88.2	0.71

Table 3. **Extended infraction analysis**. Comparison of fine-tuned LMDrive models on safety and behavior sub-metrics, averaged over V3-based configurations.

Configuration	DS ↑	RC ↑	IS ↑	CP ↓	CV ↓	CL ↓	RL ↓	SS ↓	Off ↓	RD ↓	TO ↓	AB ↓
SG00-PT	42.94	54.81	0.80	0.08	2.83	4.28	2.31	0.00	3.79	11.95	2.93	1.63
SG00-FT	41.54	48.22	0.88	0.00	0.85	2.93	0.10	0.00	2.86	9.94	4.31	2.51
SG10	48.04	56.08	0.85	0.01	1.17	2.07	2.07	0.01	2.65	8.22	2.40	2.55

CP: Collision Pedestrians, CV: Collision Vehicles, CL: Collision Layout, RL: Red Light, SS: Stop Sign, Off: Off-Road, RD: Route Deviation, TO: Timeout, AB: Agent Blocked.

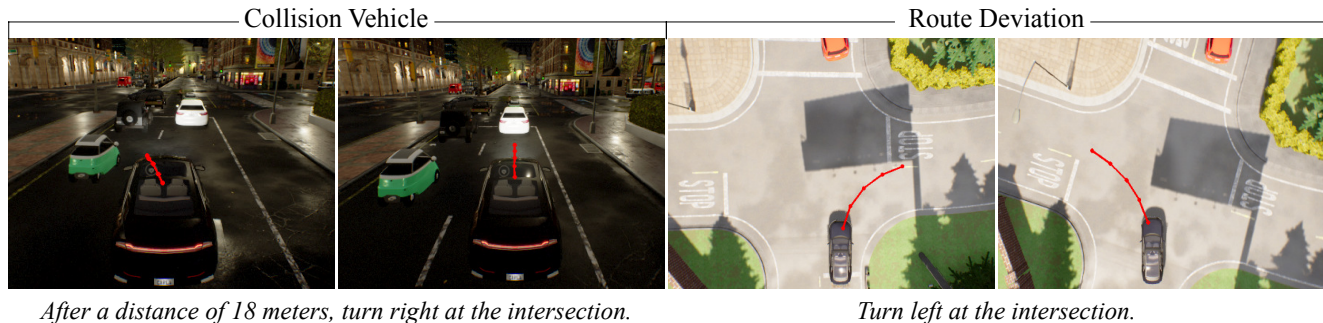


Figure 6. **Qualitative behavior comparison**. In each scenario, the LMDrive baseline (SG00-PT) on the left is compared against our SG10 on the right. The baseline predicts an unsafe lane change into traffic while failing to anticipate a right turn (Left Pair), and incorrectly turns right instead of left, whereas subsequently entering the opposite lane (Right Pair). In both scenarios, SG10 demonstrates superior command grounding and relational awareness.

ical infractions: vehicle (CV) and layout (CL) collisions drop by over 50%, while pedestrians (CP) collisions are nearly eliminated, see Fig. 6 left. Route Deviation (RD) also improves from 11.95 to 8.22, suggesting that training-time scene graph exposure fosters more structured driving even when graphs are absent at test-time. Notably, the apparent higher safety of the fine-tuned baseline (SG00-FT) in some categories (e.g. CV) is an artifact of survival bias. Its low collision rates are a consequence of poor navigational capability (RC 48.22), see Fig. 6 (right), and high timeout (TO) rates. By failing to progress, the vehicle avoids the complex traffic interactions required for route completion. In contrast, SG10 achieves the highest RC (56.08), demonstrating successful navigation through challenging scenarios, while reducing vehicle collisions by 58% relative to

the pretrained checkpoint, providing the best overall balance between safety and route adherence.

Explicit Relational Conditioning (SG11). While our primary focus is the internalization of knowledge (SG10), we additionally evaluate the impact of maintaining explicit scene graph conditioning during both training and inference (SG11). As shown in Tab. 4, the benefits of explicit test-time graphs depend on the underlying model architecture and its training protocol. For LMDrive, SG11 generally performs worse than SG10. Since we strictly adhere to the original training recipe where the LLM backbone is kept frozen, the model struggles with the distribution shift introduced by serialized scene graphs during inference, leading to performance interference. In contrast, for BEVDriver, where the LLM is updated via LoRA, SG11 (52.5 mean DS)

Table 4. **Explicit relational conditioning.** SG11 using Actor-Only graphs with V2 and V3 prompt templates.

Serialization	LMDrive						BEVDriver					
	V2			V3			V2			V3		
	DS ↑	RC ↑	IS ↑	DS ↑	RC ↑	IS ↑	DS ↑	RC ↑	IS ↑	DS ↑	RC ↑	IS ↑
SG00-PT	42.9	54.8	0.80	42.9	54.8	0.80	44.7	49.7	0.90	44.7	49.7	0.90
SG00-FT	41.5	48.2	0.88	41.5	48.2	0.88	48.9	56.4	0.86	48.9	56.4	0.86
Text	46.4	58.0	0.81	47.1	56.1	0.83	51.7	61.4	0.84	52.2	63.5	0.83
JSON	43.7	55.0	0.80	48.8	55.5	0.87	53.2	62.8	0.84	43.8	51.4	0.88
YAML	45.5	55.7	0.82	44.7	54.6	0.81	52.7	61.6	0.85	52.8	60.4	0.87
Mean	45.2	56.2	0.81	46.9	55.4	0.84	52.5	61.9	0.85	49.6	58.4	0.86

Table 5. **Noise robustness.** Evaluation of SG01 vs. SG11 under varying levels of scene graph corruption, averaged across all serialization formats for LMDrive using template V3.

Noise	SG01			SG11		
	DS	RC	IS	DS	RC	IS
None	44.7	53.8	0.83	46.9	55.4	0.84
Soft	42.4	52.1	0.82	47.1	55.2	0.84
Medium	42.4	51.4	0.83	46.1	54.7	0.82
Heavy	41.4	51.1	0.82	47.3	56.9	0.83

Table 6. **Efficiency analysis.** Impact of serialization and abstraction on tokens, latency (ms), and GPU memory (GB) using LM-Drive SG11.

Config		Tokens	Latency	GPU
Text	Full	623	107	20.9
	Road	504	93	19.6
	Actor	99	85	18.7
JSON	Full	3105	1259	39.5
	Road	2242	1066	36.0
	Actor	342	351	26.2
YAML	Full	1940	1057	32.6
	Road	1321	925	29.5
	Actor	195	254	25.1
SG00/SG10		0	57	18.3

outperforms SG10 (51.7 mean DS). In this case, the adaptive language backbone better leverages the explicit graph as a constructive reasoning scaffold. These results confirm that while the scene graph provides a valid reasoning signal across models, knowledge internalization (SG10) is a more universally robust and efficient strategy, particularly for architectures with frozen language backbones.

Scene Graph Noise Robustness. We evaluate the reliability of relational grounding by testing SG01 vs. SG11 under three noise levels (soft, medium, heavy) that simulate real-world perception and auto-labeling failures via node and edge dropout (20%–60%) as well as semantic label noise (10%–30%). As shown in Tab. 5, while the zero-

shot SG01 configuration exhibits slight degradation as noise increases, SG11 demonstrates exceptional stability, maintaining a consistent 47.3 DS even under heavy noise. This robustness is largely attributed to our use of coarse-grained spatial bins. This discretization provides a layer of symbolic abstraction that is inherently more robust to perception jitter than raw coordinates, as minor fluctuations are absorbed by the quantization buckets. While SG01 is sensitive to label swaps, SG11 learns to treat the scene graph as a relational prior rather than a literal command. During training, scene graph noise acts as a regularizer, forcing the model to cross-reference semantic labels with raw visual features. This learned multi-modal alignment allows SG11 to maintain performance by “double-checking” noisy labels against visual evidence, making the approach resilient to the corrupted or incomplete graph structures typical of real-world deployment.

Efficiency. We evaluate the computational impact of different scene graph configurations in Tab. 6. The results highlight a critical trade-off: while verbose formats such as JSON and YAML provide structured data, they incur substantial latency costs (up to 1259 ms) and GPU memory usage (39.5 GB). In contrast, the Actor-Only Text configuration remains highly efficient. Most importantly, our SG10 strategy matches the baseline (SG00) efficiency perfectly, requiring no additional tokens and maintaining a low latency of 57 ms. This confirms that SG10 provides the benefits of relational grounding with zero added computational overhead during deployment, making it the most viable solution for real-time systems.

5. Conclusion

We presented a model-agnostic training paradigm that grounds language-based autonomous driving models in explicit relational structure through serialized traffic scene graphs. By systematically evaluating different abstraction levels, serialization formats, and injection templates, we identified lightweight and effective strategies that improve driving performance without requiring architectural changes or additional training objectives. Among all con-

figurations, Actor-Only abstractions, which include only dynamic agents and their pairwise interactions, provide a strong balance between semantic relevance and token efficiency. Our experiments further revealed that scene graph prompts enhance planning behavior, even when applied only at test-time to pretrained models. More importantly, training with scene graph supervision yields additional consistent performance gains that persist even when scene graphs are removed at test-time. These findings indicate that structural priors can foster more grounded and consistent reasoning in language-based autonomous driving systems.

References

- [1] Holger Caesar, Varun Bankiti, Alex H Lang, Sourabh Vora, Venice Erin Liong, Qiang Xu, Anush Krishnan, Yu Pan, Giancarlo Baldan, and Oscar Beijbom. nuscenes: A multimodal dataset for autonomous driving. In *CVPR*, pages 11621–11631, 2020. 2
- [2] Xuesong Chen, Linjiang Huang, Tao Ma, Rongyao Fang, Shaoshuai Shi, and Hongsheng Li. Solve: Synergy of language-vision and end-to-end networks for autonomous driving. In *CVPR*, pages 12068–12077, 2025. 2
- [3] Yixiao Chen, Ruining Yang, Xin Chen, Jia He, Dongliang Xu, and Yue Yao. From static to dynamic: a survey of topology-aware perception in autonomous driving. In *ICCV*, pages 4511–4523, 2025. 1
- [4] Can Cui, Yunsheng Ma, Xu Cao, Wenqian Ye, Yang Zhou, Kaizhao Liang, Jintai Chen, Juanwu Lu, Zichong Yang, Kuei-Da Liao, et al. A survey on multimodal large language models for autonomous driving. In *WACV*, pages 958–979, 2024. 1
- [5] Daniel Dauner, Marcel Hallgarten, Tianyu Li, Xinshuo Weng, Zhiyu Huang, Zetong Yang, Hongyang Li, Igor Gilitschenski, Boris Ivanovic, Marco Pavone, et al. Navsim: Data-driven non-reactive autonomous vehicle simulation and benchmarking. *NeurIPS*, 37:28706–28719, 2024. 2
- [6] Alexey Dosovitskiy, German Ros, Felipe Codevilla, Antonio Lopez, and Vladlen Koltun. CARLA: An open urban driving simulator. In *CoRL*, pages 1–16, 2017. 2, 5
- [7] Haoyu Fu, Diankun Zhang, Zongchuang Zhao, Jianfeng Cui, Dingkan Liang, Chong Zhang, Dingyuan Zhang, Hongwei Xie, Bing Wang, and Xiang Bai. Orion: A holistic end-to-end autonomous driving framework by vision-language instructed action generation. In *ICCV*, pages 24823–24834, 2025. 2
- [8] Zhangwei Gao, Zhe Chen, Erfei Cui, Yiming Ren, Weiyun Wang, Jinguo Zhu, Hao Tian, Shenglong Ye, Junjun He, Xizhou Zhu, et al. Mini-internvl: a flexible-transfer pocket multi-modal model with 5% parameters and 90% performance. *Visual Intelligence*, 2(1):32, 2024. 5
- [9] Elias Greve, Martin Büchner, Niclas Vödisch, Wolfram Burgard, and Abhinav Valada. Collaborative dynamic 3d scene graphs for automated driving. In *ICRA*, pages 11118–11124. IEEE, 2024. 2, 3
- [10] Qiao Gu, Ali Kuwajerwala, Sacha Morin, Krishna Murthy Jatavallabhula, Bipasha Sen, Aditya Agarwal, Corban Rivera, William Paul, Kirsty Ellis, Rama Chellappa, et al. Conceptgraphs: Open-vocabulary 3d scene graphs for perception and planning. In *ICRA*, pages 5021–5028. IEEE, 2024. 1
- [11] Wencheng Han, Dongqian Guo, Cheng-Zhong Xu, and Jianbing Shen. Dme-driver: Integrating human decision logic and 3d scene perception in autonomous driving. In *AAAI*, pages 3347–3355, 2025. 2
- [12] Deepti Hegde, Rajeev Yasarla, Hong Cai, Shizhong Han, Apratim Bhattacharyya, Shweta Mahajan, Litian Liu, Risheek Garrepalli, Vishal M Patel, and Fatih Porikli. Distilling multi-modal large language models for autonomous driving. In *CVPR*, pages 27575–27585, 2025. 2
- [13] Daniel Honerkamp, Martin Büchner, Fabien Despinoy, Tim Welschehold, and Abhinav Valada. Language-grounded dynamic scene graphs for interactive object search with mobile manipulation. *IEEE Robot. Autom. Lett.*, 2024. 1
- [14] Edward J Hu, yelong shen, Phillip Wallis, Zeyuan Allen-Zhu, Yuanzhi Li, Shean Wang, Lu Wang, and Weizhu Chen. LoRA: Low-rank adaptation of large language models. In *ICLR*, 2022. 6
- [15] Jyh-Jing Hwang, Runsheng Xu, Hubert Lin, Wei-Chih Hung, Jingwei Ji, Kristy Choi, Di Huang, Tong He, Paul Covington, Benjamin Sapp, Yin Zhou, James Guo, Dragomir Anguelov, and Mingxing Tan. EMMA: End-to-end multimodal model for autonomous driving. *TMLR*, 2025. 2
- [16] Xiaosong Jia, Penghao Wu, Li Chen, Yu Liu, Hongyang Li, and Junchi Yan. Hdgt: Heterogeneous driving graph transformer for multi-agent trajectory prediction via scene encoding. *IEEE TPAMI*, 45(11):13860–13875, 2023. 1, 3
- [17] Xiaosong Jia, Zhenjie Yang, Qifeng Li, Zhiyuan Zhang, and Junchi Yan. Bench2drive: Towards multi-ability benchmarking of closed-loop end-to-end autonomous driving. *NeurIPS*, 37:819–844, 2024. 5
- [18] Justin Johnson, Ranjay Krishna, Michael Stark, Li-Jia Li, David Shamma, Michael Bernstein, and Li Fei-Fei. Image retrieval using scene graphs. In *CVPR*, pages 3668–3678, 2015. 1
- [19] Christina Kassab, Matías Mattamala, Sacha Morin, Martin Büchner, Abhinav Valada, Liam Paull, and Maurice Fallon. The bare necessities: Designing simple, effective open-vocabulary scene graphs. *arXiv preprint arXiv:2412.01539*, 2024. 1
- [20] Fanjie Kong, Yitong Li, Weihuang Chen, Chen Min, Yizhe Li, Zhiqiang Gao, Haoyang Li, Zhongyu Guo, and Hongbin Sun. Vlr-driver: Large vision-language-reasoning models for embodied autonomous driving. In *ICCV*, pages 26966–26976, 2025. 2
- [21] Junnan Li, Dongxu Li, Silvio Savarese, and Steven Hoi. Blip-2: Bootstrapping language-image pre-training with frozen image encoders and large language models. In *ICML*, pages 19730–19742, 2023. 6
- [22] Yifan Liao, Zhen Sun, Xiaoyun Qiu, Zixiao Zhao, Wenbing Tang, Xinlei He, Xinhui Zheng, Tianwei Zhang, Xinyi Huang, and Xingshuo Han. Work zones challenge vlm trajectory planning: Toward mitigation and robust autonomous driving. *arXiv preprint arXiv:2510.02803*, 2025. 3

- [23] Haotian Liu, Chunyuan Li, Yuheng Li, and Yong Jae Lee. Improved baselines with visual instruction tuning. In *CVPR*, pages 26296–26306, 2024. 5
- [24] Xinxin Liu, Yuchen Zhou, and Chao Gou. Learning from interaction-enhanced scene graph for pedestrian collision risk assessment. *IEEE T-IV*, 8(9):4237–4248, 2023. 1, 3
- [25] Changsheng Lv, Mengshi Qi, Liang Liu, and Huadong Ma. T2sg: Traffic topology scene graph for topology reasoning in autonomous driving. In *CVPR*, pages 17197–17206, 2025. 2, 3
- [26] Arnav Vaibhav Malawade, Shih-Yuan Yu, Brandon Hsu, Harsimrat Kaeley, Anurag Karra, and Mohammad Abdullah Al Faruque. roadscene2vec: A tool for extracting and embedding road scene-graphs. *Knowledge-Based Systems*, 242:108245, 2022. 2, 3
- [27] Arnav Vaibhav Malawade, Shih-Yuan Yu, Brandon Hsu, Deepan Muthirayan, Pramod P Khargonekar, and Mohammad Abdullah Al Faruque. Spatiotemporal scene-graph embedding for autonomous vehicle collision prediction. *IEEE Internet of Things Journal*, 9(12):9379–9388, 2022. 1, 3
- [28] Jianbiao Mei, Yukai Ma, Xueming Yang, Licheng Wen, Xinyu Cai, Xin Li, Daocheng Fu, Bo Zhang, Pinlong Cai, Min Dou, Botian Shi, Liang He, Yong Liu, and Yu Qiao. Continuously learning, adapting, and improving: A dual-process approach to autonomous driving. In *NeurIPS*, 2024. 2
- [29] Xiaoyu Mo, Zhiyu Huang, Yang Xing, and Chen Lv. Multi-agent trajectory prediction with heterogeneous edge-enhanced graph attention network. *IEEE Transactions on Intelligent Transportation Systems*, 23(7):9554–9567, 2022. 3
- [30] Mohammad Mohammadi, Daniel Honerkamp, Martin Büchner, Matteo Cassinelli, Tim Welschehold, Fabien Despinoy, Igor Gilitschenski, and Abhinav Valada. More: Mobile manipulation rearrangement through grounded language reasoning. *IROS*, 2025. 1
- [31] Chenbin Pan, Burhaneddin Yaman, Tommaso Nesti, Abhirup Mallik, Alessandro G Allievi, Senem Velipasalar, and Liu Ren. Vlp: Vision language planning for autonomous driving. In *CVPR*, pages 14760–14769, 2024. 2
- [32] Krishan Rana, Jesse Haviland, Sourav Garg, Jad Abou-Chakra, Ian Reid, and Niko Suenderhauf. Sayplan: Grounding large language models using 3d scene graphs for scalable robot task planning. In *CoRL*, 2023. 1
- [33] Katrin Renz, Long Chen, Elahe Arani, and Oleg Sinavski. Simlingo: Vision-only closed-loop autonomous driving with language-action alignment. In *CVPR*, pages 11993–12003, 2025. 1, 2, 5
- [34] Fabian Schmidt, Noushiq Mohammed Kayilan Abdul Nazar, Markus Enzweiler, and Abhinav Valada. Enhancing llm-based autonomous driving with modular traffic light and sign recognition. *arXiv preprint arXiv:2511.14391*, 2025.
- [35] Fabian Schmidt, Karol Fedurko, Markus Enzweiler, and Abhinav Valada. Lad-drive: Bridging language and trajectory with action-aware diffusion transformers. *arXiv preprint arXiv:2603.02035*, 2026.
- [36] Hao Shao, Yuxuan Hu, Letian Wang, Guanglu Song, Steven L Waslander, Yu Liu, and Hongsheng Li. Lmdrive: Closed-loop end-to-end driving with large language models. In *CVPR*, pages 15120–15130, 2024. 1, 2, 5
- [37] Tim Steinke, Martin Büchner, Niclas Vödisch, and Abhinav Valada. Collaborative dynamic 3d scene graphs for open-vocabulary urban scene understanding. In *IROS*, 2025. 2, 3
- [38] Xiaoyu Tian, Junru Gu, Bailin Li, Yicheng Liu, Yang Wang, Zhiyong Zhao, Kun Zhan, Peng Jia, Xianpeng Lang, and Hang Zhao. Drivevlm: The convergence of autonomous driving and large vision-language models. In *CoRL*, 2024. 2
- [39] Yafu Tian, Alexander Carballo, Ruifeng Li, and Kazuya Takeda. Rsg-gcn: Predicting semantic relationships in urban traffic scene with map geometric prior. *IEEE Open Journal of Intelligent Transportation Systems*, 4:244–260, 2023. 2, 3
- [40] Yafu Tian, Alexander Carballo, Ruifeng Li, and Kazuya Takeda. Rsg-search: semantic traffic scene retrieval using graph-based scene representation. In *2023 IEEE Intelligent Vehicles Symposium (IV)*, pages 1–8. IEEE, 2023. 3
- [41] Yafu Tian, Alexander Carballo, Ruifeng Li, Simon Thompson, and Kazuya Takeda. Rsg-search plus: An advanced traffic scene retrieval methods based on road scene graph. In *2024 IEEE Intelligent Vehicles Symposium (IV)*, pages 1171–1178. IEEE, 2024.
- [42] Yafu Tian, Alexander Carballo, Ruifeng Li, Simon Thompson, and Kazuya Takeda. Query by example: Semantic traffic scene retrieval using llm-based scene graph representation. *Sensors*, 25(8):2546, 2025. 2, 3
- [43] Hugo Touvron, Thibaut Lavril, Gautier Izacard, Xavier Martinet, Marie-Anne Lachaux, Timothée Lacroix, Baptiste Rozière, Naman Goyal, Eric Hambro, Faisal Azhar, et al. Llama: Open and efficient foundation language models. *arXiv preprint arXiv:2302.13971*, 2023. 5
- [44] Junyao Wang, Arnav Vaibhav Malawade, Junhong Zhou, Shih-Yuan Yu, and Mohammad Abdullah Al Faruque. Rs2g: Data-driven scene-graph extraction and embedding for robust autonomous perception and scenario understanding. In *WACV*, pages 7493–7502, 2024. 2, 3
- [45] Yujin Wang, Quanfeng Liu, Zhengxin Jiang, Tianyi Wang, Junfeng Jiao, Hongqing Chu, Bingzhao Gao, and Hong Chen. Rad: Retrieval-augmented decision-making of meta-actions with vision-language models in autonomous driving. In *CVPR*, pages 3838–3848, 2025. 2
- [46] Licheng Wen, Daocheng Fu, Xin Li, Xinyu Cai, Tao MA, Pinlong Cai, Min Dou, Botian Shi, Liang He, and Yu Qiao. Dilu: A knowledge-driven approach to autonomous driving with large language models. In *ICLR*, 2024. 2
- [47] Abdelrhman Werby, Chenguang Huang, Martin Büchner, Abhinav Valada, and Wolfram Burgard. Hierarchical open-vocabulary 3d scene graphs for language-grounded robot navigation. In *RSS*, 2024. 1
- [48] Katharina Winter, Mark Azer, and Fabian B Flohr. Bev-driver: Leveraging bev maps in llms for robust closed-loop driving. In *IROS*, 2025. 1, 2, 5
- [49] Shaoyuan Xie, Lingdong Kong, Yuhao Dong, Chonghao Sima, Wenwei Zhang, Qi Alfred Chen, Ziwei Liu, and Liang Pan. Are vlms ready for autonomous driving? an empirical

- study from the reliability, data and metric perspectives. In *ICCV*, pages 6585–6597, 2025. 1
- [50] Yichen Xie, Runsheng Xu, Tong He, Jyh-Jing Hwang, Katie Luo, Jingwei Ji, Hubert Lin, Letian Chen, Yiren Lu, Zhaoqi Leng, et al. S4-driver: Scalable self-supervised driving multimodal large language model with spatio-temporal visual representation. In *CVPR*, pages 1622–1632, 2025. 2
- [51] Zhenhua Xu, Yan Bai, Yujia Zhang, Zhuoling Li, Fei Xia, Kwan-Yee K Wong, Jianqiang Wang, and Hengshuang Zhao. Drivegpt4-v2: Harnessing large language model capabilities for enhanced closed-loop autonomous driving. In *CVPR*, pages 17261–17270, 2025. 2
- [52] Hang Yin, Xiuwei Xu, Zhenyu Wu, Jie Zhou, and Jiwen Lu. Sg-nav: Online 3d scene graph prompting for llm-based zero-shot object navigation. *NeurIPS*, 37:5285–5307, 2024. 1
- [53] Jianhao Yuan, Shuyang Sun, Daniel Omeiza, Bo Zhao, Paul Newman, Lars Kunze, and Matthew Gadd. Rag-driver: Generalisable driving explanations with retrieval-augmented in-context multi-modal large language model learning. In *RSS*, 2024. 2
- [54] Shuang Zeng, Xinyuan Chang, Mengwei Xie, Xinran Liu, Yifan Bai, Zheng Pan, Mu Xu, and Xing Wei. Futuresight-drive: Thinking visually with spatio-temporal cot for autonomous driving. In *NeurIPS*, 2025. 2
- [55] Jimuyang Zhang, Zanming Huang, Arijit Ray, and Eshed Ohn-Bar. Feedback-guided autonomous driving. In *CVPR*, pages 15000–15011, 2024. 2
- [56] Jiawei Zhang, Xuan Yang, Taiqi Wang, Yu Yao, Aleksandr Petiushko, and Bo Li. Safeauto: Knowledge-enhanced safe autonomous driving with multimodal foundation models. In *ICML*, 2025. 1, 2
- [57] Ruifei Zhang, Junlin Xie, Wei Zhang, Weikai Chen, Xiao Tan, Xiang Wan, and Guanbin Li. Adadrive: Self-adaptive slow-fast system for language-grounded autonomous driving. In *ICCV*, pages 5112–5121, 2025. 1, 2
- [58] Ruifei Zhang, Wei Zhang, Xiao Tan, Sibe Yang, Xiang Wan, Xiaonan Luo, and Guanbin Li. Vldrive: Vision-augmented lightweight mllms for efficient language-grounded autonomous driving. In *ICCV*, pages 5923–5933, 2025. 1, 2
- [59] Yunpeng Zhang, Deheng Qian, Ding Li, Yifeng Pan, Yong Chen, Zhenbao Liang, Zhiyao Zhang, Yingzong Liu, Jianhui Mei, Maolei Fu, Yun Ye, Zhujin Liang, Yi Shan, and Dalong Du. Graphad: Interaction scene graph for end-to-end autonomous driving. In *IJCAI*, pages 2422–2430. International Joint Conferences on Artificial Intelligence Organization, 2025. Main Track. 1, 3
- [60] Yaowen Zhang, Yi Ruan, Miaoxin Pan, Yi Yang, and Mengyin Fu. Parking-sg: Open-vocabulary hierarchical 3d scene graph representation for open parking environments. In *ICRA*, pages 7291–7297. IEEE, 2025. 2, 3
- [61] Yuchen Zhou, Xinxin Liu, Zipeng Guo, Ming Cai, and Chao Gou. Hkts: A hierarchical knowledge-guided traffic scene graph representation learning framework for intelligent vehicles. *IEEE T-IV*, pages 1–12, 2024. 3
- [62] Zikang Zhou, Luyao Ye, Jianping Wang, Kui Wu, and Kejie Lu. Hivt: Hierarchical vector transformer for multi-agent motion prediction. In *CVPR*, pages 8823–8833, 2022. 3

GraphPilot: Grounded Scene Graph Conditioning for Language-Based Autonomous Driving

Supplementary Material

This supplementary material provides additional information to support the results presented in the main paper. We include detailed implementation settings, full training-time measurements, extended quantitative results, and additional qualitative analyses. All supplementary content is intended to enhance reproducibility and provide full transparency into our experimental pipeline.

6. Implementation Details

This section provides additional details on model configuration, dataset preprocessing, and training hyperparameters for LMDrive, BEVDriver, and SimLingo. We strictly follow the official training strategies and optimization protocols provided by the respective authors for each baseline to ensure a fair and consistent comparison.

LMDrive and BEVDriver share a unified training and optimization infrastructure, as summarized in Table 7. In contrast, SimLingo utilizes a distinct training pipeline and dataset configuration, detailed in Table 8. While all models are trained across eight NVIDIA L40s GPUs, they differ in their trainable parameter subsets: LMDrive keeps the language backbone frozen, whereas BEVDriver and Sim-

Table 7. **Implementation Details for LMDrive and BEVDriver.** Both methods use their best-performing language backbones with official pretrained checkpoints (LMDrive: LLaVA-v1.5, BEVDriver: LLaMA-7B). We maintain consistent optimization hyperparameters across all experiments, though LoRA parameters apply only to the trainable language backbone of BEVDriver.

Category	Hyperparameter
Model	freeze_vit: True
	use_notice_prompt: False
	LoRA rank: 16
	LoRA alpha: 32 LoRA dropout: 0.05
Dataset	enable_start_frame_augment: True
	token_max_length: 40
	enable_notice: False
Training	Optimizer: AdamW
	lr_sched: linear_warmup_cosine_lr
	init_lr: 1e-4
	min_lr: 1e-5
	warmup_lr: 1e-6
	warmup_steps: 2000
	weight_decay: 0.06
	max_epoch: 5
batch_size_train: 1 world_size: 8	

Table 8. **Implementation Details for SimLingo.** Optimization strategy for fine-tuning the official pretrained checkpoint using InternVL2-1B as language backbone.

Category	Hyperparameter
Model	LoRA rank: 32
	LoRA alpha: 64
	LoRA dropout: 0.3
Dataset	data_module: carla_bucket_v12_dreamer
	pred_len: 11
	use_commentary: True
	use_qa: True
	qa_augmentation: True
	img_shift_augmentation: False
	hist_len: 1
	route_as: target_point_command
	use_lmdrive_commands: True
	use_old_towns: True
use_town13: True	
use_safety_flag: True	
Training	Optimizer: AdamW
	lr_sched: one_cycle_cosine
	lr: 1e-6
	warmup_steps: 5% of total steps
	weight_decay: 0.2
	betas: (0.9, 0.999)
	max_epochs: 5
	batch_size: 8 gpus: 8

Lingo utilize LoRA to update the language model. For all experiments, we use a high-performance computing cluster where each node is equipped with an AMD EPYC 9254 CPU, 384 GB RAM, and 48 GB VRAM per GPU.

7. Training Time

Our training-time analysis covers the combinations of graph abstraction level (Full, Road-Level, Actor-Only), serialization format (Text, JSON, YAML), and template version (V2, V3). We exclude V1 from this analysis, as Table 1 from the main paper shows that V1 consistently underperforms V2 and V3. Thus, to reduce computational cost, we use only the two stronger template variants for fine-tuning. Table 9 and Table 10 summarize the complete time measurements for LMDrive, BEVDriver, and SimLingo, respectively. We report total GPU time of 8 GPU nodes (see Sec. 6). In total, we conducted 42 scene graph fine-tuning runs (18 for each LMDrive and BEVDriver, 6 for SimLingo), summing up to a combined training duration of 2,797h (1,568h for LMDrive, 1,088h for BEVDriver, and 141h for SimLingo).

Table 9. **Training GPU Time Comparison.** Total GPU hours reported across serialization formats, abstraction levels, and template variants (V2, V3). As a reference, fine-tuning without scene graphs (SG00-FT) takes approx. 45h for LMDrive and 20h for BEVDriver.

Model	Serialization	Template	Full	Road-Level	Actor-Only
LMDrive	Text	V2	77h	74h	61h
		V3	77h	76h	61h
	JSON	V2	107h	105h	77h
		V3	107h	106h	78h
	YAML	V2	107h	105h	68h
		V3	106h	104h	69h
BEVDriver	Text	V2	51h	48h	34h
		V3	60h	58h	35h
	JSON	V2	78h	76h	52h
		V3	78h	76h	53h
	YAML	V2	77h	76h	43h
		V3	77h	76h	44h

Table 10. **Training GPU time for SimLingo.** GPU hours reported for all serialization formats and template variants (V2, V3) using Actor-Only abstraction. As a reference, fine-tuning without scene graph input (SG00-FT) takes approx. 19h.

Serialization	Template	Actor-Only
Text	V2	20h
	V3	21h
JSON	V2	29h
	V3	29h
YAML	V2	21h
	V3	21h

Across all models, the graph abstraction level is the dominant factor affecting training time, primarily due to differences in sequence length (see Table 1 in main paper for mean token counts). The choice of the template version has only a negligible impact, and differences between the Text and JSON/YAML serializations follow a consistent pattern: Text yields the shortest training times, while JSON and YAML are comparable but slower due to their higher structural verbosity. Similar trends hold for BEVDriver and SimLingo, although their overall training times are substantially shorter than those of LMDrive. For BEVDriver, this is attributed to the different language backbone, while SimLingo’s efficiency stems from the lightweight InternVL2-1B backbone.

8. Computational Analysis

All experiments in this section were executed on a single NVIDIA L40S GPU node (see Sec. 6). To quantify the computational overhead introduced by scene graph processing, we measure the runtime and resource usage of each compo-

nent: generation, abstraction, and serialization. These steps are evaluated across all graph abstraction levels (Full, Road-Level, Actor-Only) and serialization formats (Text, JSON, YAML) using template version V3. In addition, since test-time scene graph injection (SG01/SG11) introduces further computational costs, we also report inference latency and GPU memory usage for each configuration with LMDrive as the base model.

Table 11 presents detailed latency and memory statistics for various SG11 system configurations. Scene graph generation time remains consistent, while abstraction is only applied in Road-Level and Actor-Only configurations, contributing minimally to overall latency. Serialization time varies more significantly: Full and Road-Level abstractions require more tokens and structural elements, especially in JSON and YAML, while Actor-Only remains lightweight. Inference time is strongly influenced by both the abstraction level and the serialization format: Text is the most efficient, whereas JSON and YAML incur higher latency, particularly for Full and Road-Level abstractions due to their verbosity. This trend is also reflected in GPU memory usage. For comparison, we include the SG10 system configuration, which excludes scene graph input at test-time, resulting in the lowest overall latency and GPU usage.

9. Detailed Quantitative Results

This section provides full numerical results for all configurations evaluated in the paper. The main paper reports averaged or representative values due to space constraints; here, we include all combinations for completeness.

Extended Baseline Performance. Table 12 reports baseline results for LMDrive and BEVDriver without scene graph input (SG00), comparing pretrained (SG00-PT) and fine-tuned (SG00-FT) models across LangAuto *Tiny*, *Short*, and *Long* tracks. This table complements Table 2 from the main paper and provides full benchmark breakdowns for completeness.

Extended Zero-Shot Test-Time Scene Graph Injection (SG01). Table 13 lists complete SG01 results for LMDrive across all serialization formats, abstraction levels, and prompt templates, broken down by LangAuto benchmark track (*Tiny*, *Short*, *Long*). The results complement Table 1 from the main paper.

Extended Scene Graph-Conditioned Fine-Tuning. Table 14 and Table 15 complement Table 2 and 4 from the main paper by reporting complete benchmark-wise results for LMDrive and BEVDriver, respectively. All configurations use Actor-Only graphs and compare SG11 (train and test-time) and SG01 (test-time-only) settings across serialization formats and prompt templates V2 and V3. While the main analysis focuses on overall means, these detailed results are provided for completeness.

Table 11. **Computational analysis.** Measured latency (in milliseconds) and GPU memory usage (in GB) for each stage of the scene graph pipeline (generation, abstraction, serialization) and model inference across abstraction levels (Full, Road-Level, Actor-Only) and serialization formats (Text, JSON, YAML) under the SG11 system configuration using template V3 and LMDrive as base model. For each measurement, we report the 1st percentile (P01), median (Med), and 99th percentile (P99). The final row (SG10) serves as a baseline in which no scene graphs are used at test time, and thus no scene graph pipeline or additional token overhead is involved.

Serialization	Abstraction	Generation [ms]			Abstraction [ms]			Serialization [ms]			Latency [ms]			GPU [GB]		
		P01	Med	P99	P01	Med	P99	P01	Med	P99	P01	Med	P99	P01	Med	P99
JSON	Full	25.0	40.7	53.6	0.0	0.0	0.0	0.3	1.2	2.3	158.9	1259.2	2057.6	25.5	39.6	41.7
	Road-Level	25.8	38.6	52.8	0.1	0.2	1.1	0.4	0.9	1.9	203.9	1065.8	1967.4	23.7	36.0	41.9
	Actor-Only	25.6	39.2	54.6	0.1	0.2	1.0	0.8	1.3	2.6	288.3	351.1	516.4	23.1	26.2	29.3
YAML	Full	25.2	40.9	54.3	0.0	0.0	0.0	1.0	5.7	7.7	225.1	1056.6	1566.7	26.5	32.6	40.1
	Road-Level	25.7	41.4	54.7	0.1	0.2	0.9	1.1	4.8	7.5	287.4	924.5	1598.3	27.8	29.5	38.1
	Actor-Only	25.2	40.1	54.6	0.1	0.1	1.0	0.2	0.5	0.8	185.1	253.9	601.3	25.0	25.1	25.2
Text	Full	26.0	40.6	53.4	0.0	0.0	0.0	0.4	0.9	2.0	79.5	107.4	136.9	20.8	20.9	21.0
	Road-Level	25.3	41.4	54.0	0.1	0.2	0.4	0.2	0.8	1.6	58.1	93.3	132.3	19.6	19.6	19.8
	Actor-Only	25.4	38.7	53.6	0.1	0.1	0.3	0.2	0.5	0.7	46.4	85.4	118.9	18.2	18.7	18.9
SG10		0.0	0.0	0.0	0.0	0.0	0.0	0.0	0.0	0.0	51.6	56.9	65.5	18.2	18.3	18.4

Table 12. **Extended baseline performance.** Performance of LMDrive and BEVDriver without scene graph input during training and test-time (SG00) on different LangAuto benchmarks *Tiny*, *Short*, and *Long*. SG00-PT refers to the official pretrained checkpoints, while SG00-FT applies further fine-tuning on our collected dataset.

Method	Config	Tiny			Short			Long		
		DS \uparrow	RC \uparrow	IS \uparrow	DS \uparrow	RC \uparrow	IS \uparrow	DS \uparrow	RC \uparrow	IS \uparrow
LMDrive	SG00-PT	60.72	70.98	0.82	41.34	56.98	0.79	26.80	36.47	0.77
	SG00-FT	57.98	65.83	0.88	41.69	50.25	0.86	24.98	28.58	0.90
BEVDriver	SG00-PT	63.15	68.31	0.92	42.22	46.00	0.92	28.74	34.79	0.86
	SG00-FT	55.80	62.22	0.88	62.27	69.35	0.89	28.75	37.53	0.82

Table 13. **Extended zero-shot test-time scene graph injection (SG01).** Performance across serialization formats, graph abstraction levels, and template versions on different LangAuto benchmarks *Tiny*, *Short*, and *Long* for LMDrive using SG01 system configuration.

Serialization	Graph Abstraction	Template	Tiny			Short			Long		
			DS \uparrow	RC \uparrow	IS \uparrow	DS \uparrow	RC \uparrow	IS \uparrow	DS \uparrow	RC \uparrow	IS \uparrow
Text	Full	V1	49.6	56.0	0.87	44.7	54.1	0.85	22.5	28.5	0.81
		V2	59.3	64.4	0.89	42.1	52.8	0.83	23.9	31.0	0.77
		V3	58.5	66.5	0.86	40.0	49.5	0.84	25.3	33.1	0.79
	Road-Level	V1	54.2	60.8	0.86	43.8	52.0	0.86	23.8	28.3	0.84
		V2	58.2	64.1	0.89	43.5	54.1	0.82	22.9	30.0	0.77
		V3	58.3	64.1	0.87	41.1	56.8	0.80	22.1	29.3	0.75
	Actor-Only	V1	50.9	60.1	0.85	42.9	52.4	0.86	26.3	33.7	0.83
		V2	64.7	71.3	0.89	44.8	53.1	0.87	24.5	34.5	0.77
		V3	59.8	65.7	0.89	45.3	56.4	0.83	24.2	31.4	0.80
JSON	Full	V1	45.8	51.4	0.87	34.6	46.3	0.81	23.4	28.8	0.83
		V2	61.5	66.9	0.90	39.2	49.7	0.84	23.7	29.4	0.79
		V3	62.2	69.3	0.88	42.0	55.0	0.80	29.7	39.6	0.80
	Road-Level	V1	44.2	49.3	0.88	38.1	54.0	0.78	21.0	26.8	0.82
		V2	59.4	66.6	0.86	41.7	56.8	0.77	24.3	30.1	0.78
		V3	62.7	71.3	0.86	49.5	59.8	0.85	27.7	37.9	0.75
	Actor-Only	V1	55.6	60.8	0.89	41.5	51.0	0.86	23.9	30.1	0.81
		V2	60.2	64.7	0.91	42.7	58.1	0.78	25.0	34.1	0.76
		V3	58.7	71.0	0.82	48.0	58.1	0.86	27.5	37.5	0.77
YAML	Full	V1	49.4	54.2	0.87	47.0	54.1	0.88	21.7	28.1	0.81
		V2	60.5	66.0	0.90	41.0	54.7	0.80	23.9	30.7	0.76
		V3	56.7	62.7	0.87	43.5	58.7	0.79	25.2	34.2	0.74
	Road-Level	V1	52.3	58.0	0.87	43.1	53.8	0.86	22.3	28.0	0.82
		V2	59.3	64.8	0.90	41.4	58.3	0.77	24.8	31.6	0.79
		V3	57.9	63.8	0.88	43.5	54.4	0.84	24.9	33.7	0.77
	Actor-Only	V1	60.9	69.3	0.86	43.2	56.2	0.82	24.3	30.6	0.82
		V2	60.6	69.3	0.88	44.8	54.0	0.85	25.2	36.1	0.72
		V3	62.1	67.5	0.91	46.7	58.1	0.84	25.3	32.6	0.78

Table 14. **Extended scene graph-conditioned fine-tuning of LMDrive.** Actor-Only scene graphs with SG11 and SG01 system configuration across LangAuto benchmarks (*Tiny*, *Short*, and *Long*) for LMDrive using template versions V2 and V3.

Serialization	Template	Config	Tiny			Short			Long		
			DS \uparrow	RC \uparrow	IS \uparrow	DS \uparrow	RC \uparrow	IS \uparrow	DS \uparrow	RC \uparrow	IS \uparrow
Text	V2	SG11	66.6	76.1	0.88	45.5	60.9	0.77	27.2	36.9	0.76
		SG01	66.8	75.2	0.88	46.4	57.8	0.82	27.3	35.4	0.81
	V3	SG11	52.8	62.0	0.85	56.3	65.8	0.87	32.0	40.5	0.78
		SG01	72.6	78.7	0.91	52.9	60.6	0.87	29.9	39.0	0.81
JSON	V2	SG11	55.2	67.2	0.82	45.9	57.7	0.81	30.1	40.2	0.77
		SG01	57.7	67.6	0.86	53.3	59.7	0.88	26.1	33.2	0.81
	V3	SG11	64.9	68.6	0.94	51.1	59.1	0.84	30.5	39.0	0.82
		SG01	53.5	60.2	0.89	53.9	62.9	0.85	29.2	38.8	0.81
YAML	V2	SG11	61.3	67.1	0.90	47.5	61.2	0.79	27.8	38.8	0.75
		SG01	63.8	72.1	0.88	49.1	58.1	0.83	30.9	42.1	0.79
	V3	SG11	61.9	71.4	0.86	43.7	53.7	0.79	28.6	38.8	0.77
		SG01	63.7	71.0	0.89	50.9	56.8	0.87	25.8	36.8	0.75

Table 15. **Extended scene graph-conditioned fine-tuning of BEVDriver.** Actor-Only scene graphs with SG11 and SG01 system configuration across LangAuto benchmarks (*Tiny*, *Short*, and *Long*) for BEVDriver using template versions V2 and V3.

Serialization	Template	Config	Tiny			Short			Long		
			DS \uparrow	RC \uparrow	IS \uparrow	DS \uparrow	RC \uparrow	IS \uparrow	DS \uparrow	RC \uparrow	IS \uparrow
Text	V2	SG11	60.7	69.0	0.88	59.2	71.5	0.83	35.2	43.7	0.81
		SG01	66.9	78.5	0.85	50.0	54.5	0.93	38.2	46.5	0.83
	V3	SG11	61.5	71.1	0.88	60.8	70.4	0.88	34.2	49.0	0.73
		SG01	61.3	67.8	0.90	59.5	67.8	0.89	33.7	44.4	0.78
JSON	V2	SG11	60.9	69.4	0.88	63.9	73.3	0.88	34.7	45.7	0.76
		SG01	52.0	57.1	0.89	54.9	58.5	0.94	35.1	40.7	0.85
	V3	SG11	49.3	56.3	0.89	47.2	55.0	0.90	34.9	43.0	0.83
		SG01	49.2	56.9	0.90	48.4	55.9	0.89	29.1	39.3	0.77
YAML	V2	SG11	58.0	64.0	0.91	64.1	72.8	0.87	36.1	48.1	0.78
		SG01	58.8	69.2	0.86	71.7	76.2	0.94	37.7	46.8	0.81
	V3	SG11	58.4	67.8	0.86	58.5	63.6	0.90	41.7	49.7	0.84
		SG01	58.8	66.4	0.86	55.3	62.9	0.87	30.5	37.7	0.81

10. Qualitative Results

Alongside this supplementary material, we include a video providing a brief overview of our method and a comparison of the different scene graph abstraction levels (Full, Road-Level, and Actor-Only) for a representative driving scenario. We then showcase qualitative results for each of the three evaluated architectures LMDrive, BEVDriver, and SimLingo. The video highlights specific scenarios where the original pretrained baselines (SG00-PT) fail due to collisions or incorrect instruction following, and demonstrates how our scene graph-conditioned models (SG10) successfully navigate these challenges through internalized relational reasoning.